From scalar to string confinement

Theodore J. Allen*
SUNY Institute of Technology, School of Arts & Sciences, P.O. Box 3050, Utica, New York 13504

M. G. Olsson
Department of Physics, University of Wisconsin, 1150 University Avenue, Madison, Wisconsin 53706

Siniša Veseli
Fermi National Accelerator Laboratory, P.O. Box 500, Batavia, Illinois 60510
(Received 25 January 2000; published 9 October 2000)

We outline a connection between scalar quark confinement, a phenomenologically successful concept heretofore lacking fundamental justification, and QCD. Although scalar confinement does not follow from QCD, there is an interesting and close relationship between them. We develop a simple model intermediate between scalar confinement and the QCD string for illustrative purposes. Finally, we find analytically the bound state spectrum of the light degrees of freedom for a spinless, massless quark in scalar, time-component vector, and string confinement through semi-classical quantization.

PACS number(s): 12.38.Aw

I. INTRODUCTION

Going beyond the non-relativistic potential model of quark confinement means that more than the static interaction energy must be specified. In the language of potential models the Lorentz nature of the interaction is needed. To agree with the observed spin-orbit splitting it was proposed long ago [1] that the large distance (confining) potential is a Lorentz scalar. In this case there is no magnetic field to influence the quarks' spins and the only spin-orbit interaction is the kinematic ''Thomas term.'' The Thomas type spin-orbit interaction partially cancels that of the short range one-gluon exchange, in agreement with the observed spectrum [2].

Some insight into the use of the scalar potential was given by Buchmüller [3]. His argument is that at large distances one expects the QCD field of the quarks to become string- or flux-tube-like. The QCD flux tube is purely chromoelectric in its rest frame, and hence in the rest frame of each quark there is no chromomagnetic field to provide a spin-orbit interaction. The scalar interaction yields this same result by fiat; there is no magnetic field anywhere because it is not a vector-type interaction. This provides some justification for using the scalar potential but does not establish a direct connection. It agrees only in having the same spin-orbit interaction at long range as QCD.

Subsequently it was shown that for slowly moving quarks QCD predicts both spin-dependent [4] and spin-independent [5] relativistic corrections. The long-range spin dependence is just the Thomas type spin-orbit interaction [6].

The spin-independent QCD corrections differ from those of scalar confinement [7,8]. It also has been established that the QCD predictions at long distance are the same as those of a string or flux tube interaction [8]. Lattice simulations also favor the Thomas interaction [9]. The current state of lattice simulations is reviewed in Ref. [10].

Since spin-independent effects are difficult to identify from the experimental data, scalar confinement remains phenomenologically successful. As scalar confinement is also relatively simple computationally, it continues to be a popular and useful tool in hadron physics. It should be pointed out that its use in the Salpeter equation leads to cancellations [11] in the ultra-relativistic limit, resulting in a very non-linear Regge trajectory [11–13].

Although scalar confinement has been used for a long time in hadron physics, its relation to QCD has never been clarified. It is the purpose of this paper to place scalar confinement in relation to QCD and in particular to the QCD string. In Sec. II we point out that there is a certain four-vector potential that is isomorphic to a scalar potential. In Sec. III we compare this four-vector potential to the QCD string. Noting certain similarities and differences, we propose a model intermediate between the string and scalar confinement. The semi-relativistic reductions for scalar, time-component vector, intermediate, and string confinements are compared in Sec. IV. Although by construction, all these confinement models have the same non-relativistic limit, their relativistic reductions differ. In Sec. V we explore the ''ultra-relativistic'' Regge sector with a massless quark via semi-classical quantization. The Regge behavior of the different confinement models show some remarkable similarities and differences. Finally, in Sec. VI we present our conclusions and summarize our work.

II. THE FOUR-VECTOR POTENTIAL ISOMORPHIC TO THE SCALAR POTENTIAL

The action for a scalar (spinless) quark moving in Lorentz scalar and four-vector potentials, $\phi(x)$, and $A_\mu(x)$ respectively, is

$$S=-\int d\tau\,[m+\phi(x)-u^\mu A_\mu(x)], \tag{2.1}$$

*Present address: Department of Physics, Hobart and William Smith Colleges, Geneva, NY 14456.

where m is the rest-mass of the quark, u^μ is the quark's four-velocity, and $d\tau$ is the proper time element dt/γ. The quark four-velocity, $u^\mu=(\gamma,\gamma\mathbf{v})$, with $\gamma=(1-\mathbf{v}^2)^{-1/2}$, satisfies $-u^\mu u_\mu=1$.

When $A_\mu(x)\equiv 0$, the action (2.1) reduces to the usual scalar potential action. On the other hand, when $\phi(x)=0$, the action (2.1) describes a quark moving in an ''electromagnetic'' $[U(1)\subset SU(3)_{\text{color}}]$ color field. It was pointed out by Buchmüller [3] that in the rest frame of the QCD flux tube there is no color magnetism so that the only spin orbit interaction is Thomas precession. If we want to implement Buchmüller's criterion we may assume [14] that in the quark rest frame

$$A^{\mu'}(x)=(\phi(r),\mathbf{0}), \tag{2.2}$$

where $\phi(r)\equiv A^{0'}(x)$ is the time component of $A^{\mu'}(x)$. In the laboratory frame, where the quark velocity is $\mathbf{v}$, the four-vector potential is

$$A^\mu=u^\mu\phi(r)=(\gamma,\gamma\mathbf{v})\phi(r). \tag{2.3}$$

We note that the components depend on both position and velocity. The vector potential contributes to the action (2.1) as

$$u^\mu A_\mu=-\phi(r). \tag{2.4}$$

The resulting contribution is exactly the same as the scalar potential in Eq. (2.1). The four-vector potential corresponding to $\phi(r)=ar$ was discussed by us earlier in Ref. [14].

By this simple demonstration we have shown that there are two Lorentz type potentials that have identical consequences. The four-vector version is apparently more closely related to gauge theories like QCD. As we will see, we can quite closely draw similarities and differences.

III. COMPARING SCALAR AND STRING CONFINEMENT—AN INTERMEDIATE MODEL EMERGES

For a spinless quark moving relative to a heavy quark at the origin, the action can be written as the time integral of a function of the light quark's position and velocity,

$$S=\int dt\,L(\mathbf{r},\mathbf{v}). \tag{3.1}$$

If we consider the quark as a particle of mass m moving in a linear scalar confining potential $\phi(r)=ar$, its Lagrangian is

$$L_{\text{scalar}}=-\gamma^{-1}(m+\phi(r))=-m\sqrt{1-v^2}-ar\sqrt{1-v^2}. \tag{3.2}$$

At large distances, QCD is thought to resemble a Nambu-Goto string or flux tube model. For a scalar quark at the end of a straight flux tube, the corresponding Lagrangian is [15]

$$L_{\text{string}}=-m\sqrt{1-v^2}-ar\int_0^1 d\sigma\sqrt{1-\sigma^2v_\perp^2}, \tag{3.3}$$

where $v_\perp$ is the quark velocity transverse to the string. Comparing the scalar and string interactions, we see there are two evident differences. The first is that the string energy is spread along the length of the string whereas in the scalar potential case the energy may be thought of as being concentrated at the quark coordinate. The second is that because of the reparametrization invariance of the Nambu-Goto action (which physically is the invariance of an electric field to boosts along its direction), from which Eq. (3.3) follows, only the transverse velocity of the string may appear in the interaction energy.

The first distinction can be considered as a quantitative one which leaves the basic structure unchanged. This difference changes the velocity dependence of the additional three-momentum due to the interaction from $\mathbf{p}=ar\mathbf{v}$ in the scalar case to $\mathbf{p}=(ar/2v_\perp)[\arcsin v_\perp/v_\perp-\sqrt{1-v_\perp^2}]\hat{\mathbf{v}}_\perp$ for the string.

The second distinction has far-reaching consequences. In a non-rotating (s-wave) system, the scalar interaction contributes to the momentum whereas the string does not. The string Hamiltonian contributes only as the time component of a vector potential (vector-like) while the scalar Hamiltonian remains scalar.

It is instructive to construct a confinement model in which one of the above distinctions is removed. We will briefly consider the intermediate model having Lagrangian

$$L_{\text{int}}=-m\sqrt{1-v^2}-ar\sqrt{1-v_\perp^2}. \tag{3.4}$$

We note that although the interaction is concentrated at the quark position, it depends only on the transverse velocity.

This Lagrangian will lead to a Hamiltonian having characteristics of the string while remaining algebraically tractable.

In the usual way, the Hamiltonian corresponding to Eq. (3.4) is found to be

$$H_{\text{int}}=m\gamma+ar\gamma_\perp, \tag{3.5}$$

and the angular momentum, $J=\partial L_{\text{int}}/\partial\omega$, with $v_\perp=\omega r$, is

$$J=m\gamma v_\perp r+ar^2\gamma_\perp v_\perp. \tag{3.6}$$

Unlike in the string system, the velocities here can be eliminated in favor of the momenta, making this model much more tractable. From the definition of radial momentum

$$p_r=\frac{\partial L_{\text{int}}}{\partial\dot{r}}=m\gamma\dot{r}, \tag{3.7}$$

the useful identity

$$m\gamma=W_r\gamma_\perp, \tag{3.8}$$

with

$$W_r\equiv\sqrt{p_r^2+m^2}, \tag{3.9}$$

follows.

Using the identity (3.8), we find that $H_{\rm int}$ and J of Eqs. (3.5), (3.6) become

$$H_{\rm int}=(W_r+ar)\gamma_\perp, \tag{3.10}$$

$$J=rv_\perp\gamma_\perp(W_r+ar). \tag{3.11}$$

We can solve Eq. (3.11) for $\gamma_\perp$ using $v_\perp^2=1-\gamma_\perp^{-2}$, and substituting into Eq. (3.10) to obtain

$$H_{\rm int}=\sqrt{\frac{J^2}{r^2}+(W_r+ar)^2}. \tag{3.12}$$

IV. COMPARING RELATIVISTIC CORRECTIONS OF SPINLESS CONFINEMENT MODELS

As we have seen, there are several types of confinement models, even for spinless quarks. In this section we will enumerate and compare the relativistic reductions of various models. We first consider the relativistic reductions of the classic static potential models.

A. Scalar confinement

From the scalar interaction Lagrangian (3.2) with $\phi=ar$, we find the canonical three-momentum to be

$$\mathbf{p}=(m+ar)\gamma\mathbf{v}, \tag{4.1}$$

which results in the Hamiltonian

$$H=\sqrt{p^2+(m+ar)^2}. \tag{4.2}$$

For $m\gg ar$ and $m\gg p$, we expand to obtain the relativistic corrections

$$\begin{aligned}H&\simeq\sqrt{p^2+m^2}+ar-\frac{a}{2m^2}p^2r+\cdots\\&=\sqrt{p^2+m^2}+ar-\frac{ap_r^2r}{2m^2}-\frac{aJ^2}{2m^2r}+\cdots.\end{aligned} \tag{4.3}$$

Even though scalar confinement will yield, for spin-1/2 quarks, the spin-orbit interaction consistent with experiment, lattice QCD simulations [9], and QCD in the low velocity Wilson loop approach [5], the spin-independent terms in Eq. (4.3) are inconsistent with QCD [5,7,8].

B. Time component vector confinement

In time component vector confinement models, the potential ar is taken to be the (laboratory frame) time component of a vector potential A^μ; $A^\mu=(ar,\mathbf{0})$. The quark Lagrangian then is

$$L_{\rm vector}=-m\sqrt{1-v^2}-ar. \tag{4.4}$$

The canonical three-momentum following from this Lagrangian,

$$\mathbf{p}=\boldsymbol{\nabla}_{\mathbf{v}}L=m\gamma\mathbf{v}, \tag{4.5}$$

leads to the Hamiltonian

$$H=\sqrt{m^2+p^2}+ar. \tag{4.6}$$

There are no relativistic corrections other than kinetic energy corrections. Vector confinement is disfavored since the associated spin-orbit interaction adds to the short range spin-orbit interaction giving spin-orbit splittings that are too large when compared to experimental values [1,2] or lattice simulations [10].

The lack of spin-independent relativistic corrections is also inconsistent with the low velocity Wilson loop expansion of QCD [5].

C. Intermediate model

The Hamiltonian for this model was given in Eq. (3.12). The relativistic reduction for $m\gg ar$ and $m\gg p$ is

$$H_{\rm int}\simeq\sqrt{p^2+m^2}+ar-\frac{aJ^2}{2m^2r}+\cdots. \tag{4.7}$$

Comparing to $H_{\rm scalar}$ in Eq. (4.3), we see the same reduction except for the missing p_r term. This might be expected since the interaction does not contribute to the radial momentum. We discuss this result further in the following subsection.

D. String confinement

The reduction of the string is discussed in Ref. [8], where it was shown that the string contributes a rotational energy equal to that of a uniform rod of length r and mass ar. This energy is

$$E_R=\frac{1}{2}I\omega^2=\frac{1}{2}k(ar)r^2\left(\frac{J}{mr^2}\right)^2=\frac{kaJ^2}{2m^2r}, \tag{4.8}$$

where the geometrical factor $k=\frac{1}{3}$ for a uniform rod. If all of the ''mass'' of the string is concentrated at the position of the moving quark end, then $k=1$.

The ''kinetic'' energy term, when expanded, yields

$$\sqrt{p^2+m^2}\simeq m+\frac{p^2}{2m}-\frac{p^4}{8m^3}+\cdots. \tag{4.9}$$

In the semi-relativistic regime the momentum is mostly that of the quark with a small contribution from the ''interaction:''

$$\begin{aligned}p^2&=p_r^2+\frac{1}{r^2}(J_q+J_{\rm in})^2\\&\simeq\left(p_r^2+\frac{J_q^2}{r^2}\right)+\frac{2J_qJ_{\rm in}}{r^2}\simeq p_q^2+\frac{2J_q}{r^2}\left(\frac{J_q}{mr^2}\right)(kar^3),\end{aligned} \tag{4.10}$$

$$p^2\simeq p_q^2+4mE_R, \tag{4.11}$$

and hence

$$\sqrt{p^2+m^2} \simeq \sqrt{p_q^2+m^2}+2E_R. \tag{4.12}$$

So, if one separates the Hamiltonian into the quark's energy plus an interaction energy $ar+E_R$, then

$$H \simeq \sqrt{p^2+m^2}+ar-E_R. \tag{4.13}$$

This is exactly what one finds in the intermediate models where $k=1$. The string Hamiltonian is then the same, only with $k=\frac{1}{3}$:

$$H \simeq \sqrt{p^2+m^2}+ar-\frac{aJ^2}{6m^2r}. \tag{4.14}$$

This result follows systematically from the string invariants (5.18) and (5.19) in the large mass expansion [8].

V. COMPARING REGGE STRUCTURES OF SPINLESS CONFINEMENT MODELS

In this section we explore both the analytic and the numerical solutions for the Regge spectroscopy expected from the previously considered models. In particular, we investigate the ultra-relativistic limit when the ''light'' quark has zero mass. The extension to two light quarks is straightforward. It is in this ''massless'' limit where straight Regge trajectories with evenly spaced daughter trajectories are obtained in many confinement models and a close correspondence to observed light and heavy-light mesons is expected. In our analytical work we will usually assume that the orbital excitations are large compared to the radial excitation. We may consequently expect the semi-classical quantization scheme to be quite accurate. Quantization is carried out by performing the phase-space integral,

$$2\pi(n+\Gamma) = \oint p_r\, dr = 2\int_{r_-}^{r_+} p_r\, dr, \tag{5.1}$$

where $r_\pm$ are the classical turning points and Γ is a constant that depends upon the problem.[1] As shown by Langer [16], the classical angular momentum J must be replaced by $J+\frac{1}{2}$ in the expression for the radial momentum p_r.

In all cases considered here, the quantization integral can be written, or accurately approximated by

$$\int_{r_-}^{r_+} p_r\, dr = C\int_{y_-}^{y_+} \frac{dy}{y}\sqrt{(y_+-y)(y-y_-)}, \tag{5.2}$$

where y is either r or r^2 and C is a constant. This integral can be carried out to yield the the semi-classical quantization relation

$$n+\Gamma = \frac{C}{2}[y_++y_--2\sqrt{y_+y_-}]. \tag{5.3}$$

[1]Roughly, Γ depends on the nature of the potential at the turning point. For two smooth turning points $\Gamma=\frac{1}{2}$, and for two rigid walls $\Gamma=1$. For the mixed case of one of each, $\Gamma=\frac{3}{4}$.

A. Scalar confinement

We first consider the scalar case because of its simplicity and its central role in this paper. The square scalar Hamiltonian, Eq. (4.3), with the light quark massless is

$$H^2 = p^2+a^2r^2. \tag{5.4}$$

This is equivalent to the three-dimensional harmonic oscillator and its eigenvalues are well known to be

$$M^2 = 2a\left(J+2n+\frac{3}{2}\right), \quad J,n=0,1,2,3,\ldots, \tag{5.5}$$

where J is now the angular momentum quantum number. To connect with the analytic solutions to the remaining confinement models we compute the semi-classical solution for this interaction.

Semi-classical quantization starts with the separation of the momentum into angular and radial pieces, $p^2=p_r^2+J^2/r^2$, and hence

$$p_r^2 = M^2-\frac{J^2}{r^2}-a^2r^2. \tag{5.6}$$

The classical turning points ($p_r=0$) satisfy

$$r_+^2+r_-^2 = \left(\frac{M}{a}\right)^2,$$

$$r_+r_- = \frac{J}{a}, \tag{5.7}$$

$$\frac{a}{r}\sqrt{(r_+^2-r^2)(r^2-r_-^2)} = p_r.$$

Comparing this last relation to Eq. (5.2), we read off $C=a/2$, and $y=r^2$, and by Eq. (5.3) with $\Gamma=\frac{1}{2}$ and $J\to J+\frac{1}{2}$, we find

$$n+\frac{1}{2} = \frac{a}{4}\left[\frac{M^2}{a^2}-\frac{2}{a}\left(J+\frac{1}{2}\right)\right], \tag{5.8}$$

which yields

$$M^2 = 2a\left[J+2n+\frac{3}{2}\right], \tag{5.9}$$

identical to the exact solution (5.5).

In Fig. 1 we show the Regge plot for pure scalar confinement. The dots represent the exact numerical solution by the variational method, for instance see the appendix in Ref. [11]. The numerical solutions correspond to the unsquared Hamiltonian (4.2) with $m=0$. The lines are the analytic solution, Eq. (5.5) or (5.9). We note that states of even (or odd) J are degenerate. This is unique among combinations of scalar and time-component vector potential confinement [17].

It is important to note that the ''ultra-relativistic'' limit where the quark mass vanishes is in fact not ultra-relativistic

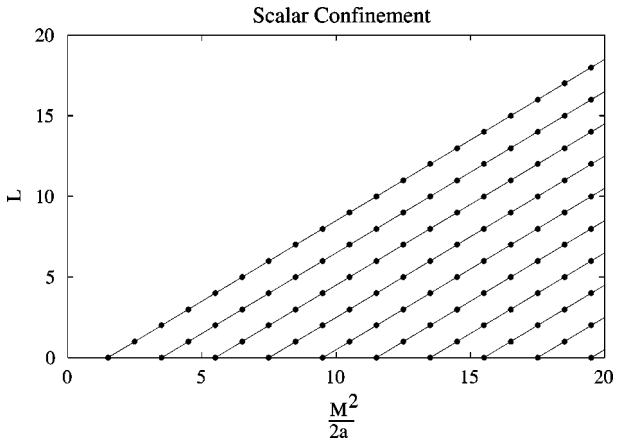

FIG. 1. Regge structure and states in pure linear scalar confinement from numerical diagonalization of the Hamiltonian (4.2) with $m=0$. Solid lines are the semi-classical result, which is exact for the squared Hamiltonian (5.4).

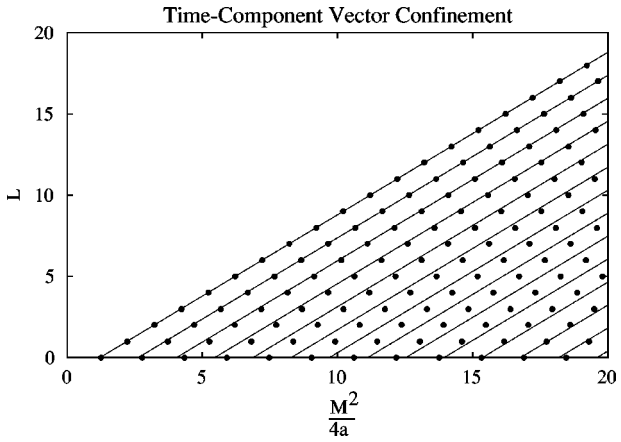

FIG. 2. Regge structure and states in pure linear time-component vector confinement from numerical diagonalization of the Hamiltonian in Eq. (4.6) with $m=0$. Solid lines are the approximate semi-classical result of Eq. (5.17).

for scalar confinement. From the Hamiltonian (5.4) with $p^2=p_r^2+J^2/r^2$, the circular orbit condition is

$$\left.\frac{\partial H^2}{\partial r}\right|_J=0, \tag{5.10}$$

which implies a circular orbit radius of

$$r_0^2=\frac{J}{a}. \tag{5.11}$$

The circular velocity is then given by

$$v_{\perp 0}=r_0\left.\frac{\partial H}{\partial J}\right|_{r=r_0}=\frac{1}{\sqrt{2}}. \tag{5.12}$$

The massless quark moves at a velocity less than unity because the scalar interaction contributes an effective mass of ar_0.

B. Time-component vector confinement

The Hamiltonian (4.6), with $m=0$ and the replacement $p^2=p_r^2+J^2/r^2$, becomes

$$p_r^2=(M-ar)^2-\frac{J^2}{r^2}=\left(M-ar-\frac{J}{r}\right)\left(M-ar+\frac{J}{r}\right). \tag{5.13}$$

The first factor contains the classical turning points and the second has only distant zeros. To good approximation, we may use the zero condition $M-ar=J/r$ from the first term in the second, and obtain

$$p_r^2\simeq\frac{2Ja}{r^2}\left(-r^2+\frac{M}{a}r-\frac{J}{a}\right). \tag{5.14}$$

This is of the form of our general phase-space integrand in Eq. (5.2) with $C=\sqrt{2Ja}$, $y=r$, where the turning points satisfy

$$r_++r_-=\frac{M}{a},$$

$$r_+r_-=\frac{J}{a}. \tag{5.15}$$

The quantization condition, Eq. (5.3), becomes

$$n+\frac{1}{2}=\frac{\sqrt{2Ja}}{2}\left[\frac{M}{a}-2\sqrt{\frac{J}{a}}\right]. \tag{5.16}$$

Solving for M^2, dropping the small squared radial excitation energy and making Langer's replacement of J by $J+\frac{1}{2}$, we find

$$M^2=4a\left(J+\sqrt{2}n+\frac{1}{2}+\frac{1}{\sqrt{2}}\right). \tag{5.17}$$

Figure 2 shows the Regge spectrum of time component vector confinement. The semi-classical quantization method yields the correct slope, radial excitation energy, and even nearly the correct $J=0$ intercept.

C. Intermediate model

From the intermediate model Hamiltonian, Eq. (3.12), the Regge spectrum can be exactly computed numerically, which we show in Fig. 3. The Regge trajectories are neither straight, nor equally spaced. The radial excitation energy is several times larger than the scalar confinement potential. A comparison of the intermediate and scalar Hamiltonians reveals that they coincide in the classical circular orbit limit. It is in radial excitation that the two models differ qualitatively. Of course, even the quantized $n=0$ radial state has some radial excitation. A semi-classical quantization can also be done in this case and yields a complicated transcendental relationship between M^2 and J.

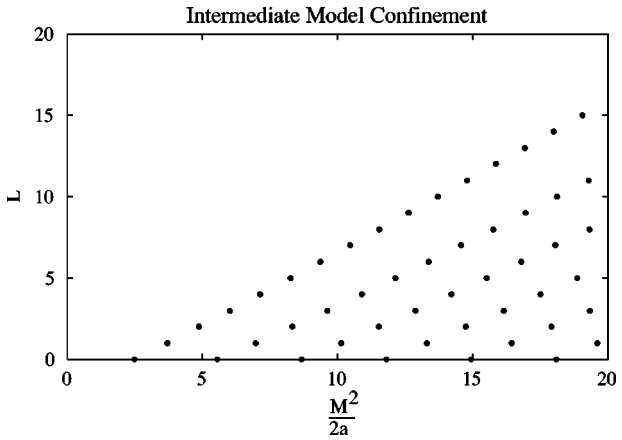

FIG. 3. States in pure intermediate model linear confinement from numerical diagonalization of the Hamiltonian (3.12) with $m=0$.

D. String confinement

In this subsection we find that the Regge structure of the confining string, with a massless quark at its end, resembles almost exactly scalar confinement once the energy is rescaled. This, despite the anomalous Regge trajectories of the ''intermediate'' model which was supposed to mimic the string. We will later discuss the reason for the occurrence. We begin with the string Lagrangian (3.3). The conserved quantities H and $J=\partial L/\partial\omega$ are [18]

$$\frac{J}{r}=W_r\gamma_\perp v_\perp+\frac{ar}{2v_\perp}\left(\frac{\arcsin v_\perp}{v_\perp}-\sqrt{1-v_\perp^2}\right), \tag{5.18}$$

$$H=W_r\gamma_\perp+ar\frac{\arcsin v_\perp}{v_\perp}, \tag{5.19}$$

where the ''radial energy'' $W_r=\sqrt{p_r^2+m^2}$ was defined in Eq. (3.9) and $v_\perp=\omega r$. For circular orbits in the massless quark limit the end of the string approaches the speed of light ($v_\perp\to 1$). Since this is the limit we are interested in for the Regge structure we set $v_\perp=1$ in the string quantities in Eq. (5.18) and (5.19) to obtain

$$\frac{J}{r}=W_r\gamma_\perp v_\perp+\frac{a\pi r}{4}, \tag{5.20}$$

$$H=W_r\gamma_\perp+\frac{a\pi r}{2}. \tag{5.21}$$

We do not set $v_\perp=1$ in the quark terms since a delicate limiting process occurs. In this limit, all of the angular momentum and energy resides in the string and all of the radial momentum is carried by the quark.

Next, we consider the difference of the squares of H and J/r

$$H^2-\frac{J^2}{r^2}=W_r^2+\frac{a\pi r}{2}W_r\gamma_\perp+\frac{3}{4}\left(\frac{a\pi r}{4}\right)^2. \tag{5.22}$$

Using Eq. (5.20) to eliminate $W_r\gamma_\perp$, after a little simplification we find

$$H^2=p_r^2+\frac{J^2}{r^2}+\frac{a\pi J}{2}+\left(\frac{a\pi r}{4}\right)^2, \tag{5.23}$$

where $W_r^2=p_r^2$ in the massless limit.

If we define

$$H_0^2=H^2-\frac{a\pi J}{2}, \tag{5.24}$$

$$a_0=\frac{\pi a}{4}, \tag{5.25}$$

the square of the string Hamiltonian appears to be a harmonic oscillator

$$H_0^2=p_r^2+\frac{J^2}{r^2}+a_0^2r^2, \tag{5.26}$$

which is very similar in form to the squared scalar confinement Hamiltonian (5.4).

The squared string Hamiltonian in Eq. (5.23) has a critical difference from the harmonic oscillator, as we now demonstrate. The circular orbit occurs where

$$\left.\frac{\partial H^2}{\partial r}\right|_J=0, \tag{5.27}$$

which implies that the circular orbit radius is

$$r_0^2=\frac{4J}{a\pi}. \tag{5.28}$$

The associated circular orbit velocity is

$$v_{\perp 0}=r_0\,\omega=r_0\left.\frac{\partial H}{\partial J}\right|_{r=r_0}=1. \tag{5.29}$$

Thus, as we mentioned previously, the massless quark moves at the speed of light in a circular orbit. For radial excitation the quark moves in the effective potential of Eq. (5.23).

From the limiting form (5.20) of the angular momentum (5.18), we see that for radial motion the radius cannot exceed r_0 because $W_r\gamma_\perp v_\perp$ cannot be negative. The $r=r_0$ coordinate represents a horizon or ''impenetrable barrier'' and the quark moves in the ''half harmonic oscillator'' potential shown in Fig. 4.

The semi-classical quantization of the string motion is equivalent to a half harmonic oscillator shifted by an amount $a\pi J/2=2a_0J$. The half harmonic quantization condition is

$$\pi\left(n+\frac{3}{4}\right)=\frac{a_0}{2}\int_{y_-}^{y_0}\frac{dy}{y}\sqrt{(y_+-y)(y-y_-)}, \tag{5.30}$$

where $y=r^2$, $y_0=r_0^2$, and $\Gamma=\frac{3}{4}$, corresponding to one smooth turning point. The integral is not precisely one-half

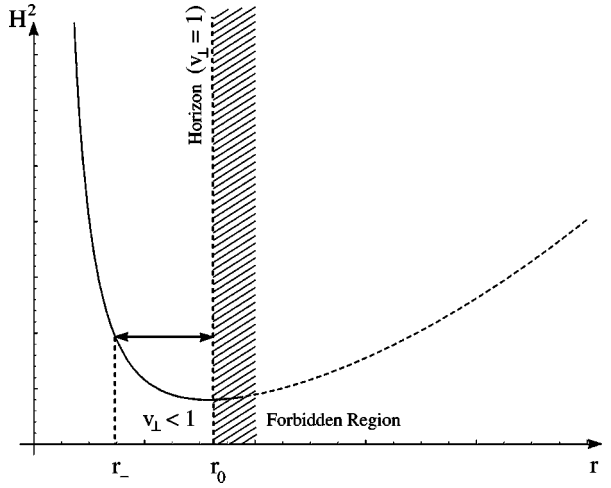

FIG. 4. Potential for the half-harmonic oscillator seen by a massless quark on string, Eq. (5.26). The horizon is at the minimum of the potential. The classical turning points are r_- and r_0.

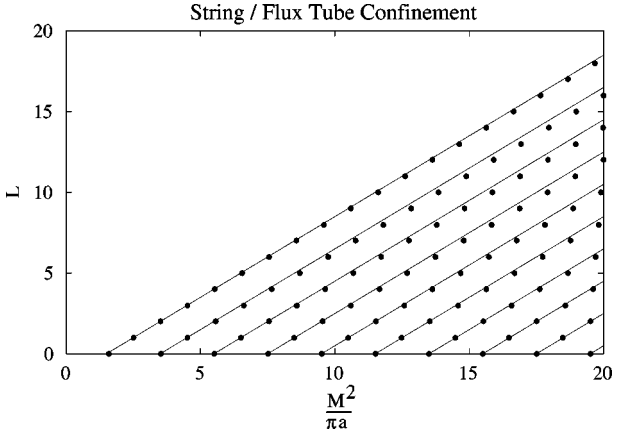

FIG. 5. Regge structure and states in string confinement from numerical quantization of Eqs. (5.18) and (5.19). Solid lines are the approximate semi-classical result of Eq. (5.33) with intercept $\frac{3}{2}$ as given in Eq. (5.36).

of the full harmonic oscillator integral but the difference vanishes for large J. The result is

$$\pi\left(n+\frac{3}{4}\right)=\frac{\pi}{8a_0}\left[M_0^2-2a_0\left(J+\frac{1}{2}\right)\right], \tag{5.31}$$

or

$$M_0^2=2a_0\left(J+4n+\frac{3}{4}+\frac{1}{2}\right). \tag{5.32}$$

Finally, we rewrite Eq. (5.32) in terms of $M^2=M_0^2+a\pi J/2$ and $a=4a_0/\pi$ to obtain

$$M^2=a\pi\left(J+2n+\frac{7}{4}\right). \tag{5.33}$$

We observe that the combination of the shift and the half oscillator reproduces the $J+2n$ pattern of excitation seen in the harmonic oscillator, and hence in scalar confinement.

We can check the intercept ($J=0$) by directly quantizing the s-wave states. From Eq. (5.19) with $\gamma_\perp=1$, we have

$$H=p_r+ar\equiv M. \tag{5.34}$$

The quantization integral,

$$\pi\left(n+\frac{1}{2}\right)=\int_0^{M/a}dr(M-ar)=\frac{M^2}{a}-\frac{M^2}{2a}, \tag{5.35}$$

directly yields

$$M^2=\pi a\left(2n+1+\frac{1}{2}\right), \tag{5.36}$$

where the $\frac{1}{2}$ is the Langer correction for the radial equation. The result indicates the 3D harmonic oscillator. We conclude that the true intercept that should appear in Eq. (5.33) ought to lie between $\frac{3}{2}$ and $\frac{7}{4}$. In Fig. 5 we show the exact numerical string Regge excitations with quark mass $m=0$. The numerical solutions of Eqs. (5.18) and (5.19) have been discussed earlier [18]. The lines are the analytic solution (5.33) but with intercept $\frac{3}{2}$ from Eq. (5.36). Similar solutions obtained from different points of view have been obtained previously [19].

VI. CONCLUSIONS AND SUMMARY

The concept of scalar confinement has been an important ingredient in hadron model building for over two decades. Its primary motivation was the resulting pure Thomas type spin-orbit interaction which partially cancels the vector type short range spin-orbit contributions. Despite its phenomenological success, scalar confinement has always had an uncertain relationship with fundamental theory. As pointed out by Buchmüller [3], the desired spin terms follow if the color magnetic field vanishes in the quark rest frame. This situation assumes no interaction with the quark color magnetic moment and occurs naturally in the usual color electric flux tube expected from QCD. This observation originally was proposed to justify the use of scalar confinement [3]. We emphasize here that this does not imply that the scalar potential follows from QCD, only that they share a common spin-orbit interaction.

In this paper we have demonstrated that a four-vector confinement interaction we found previously [14] is equivalent to scalar confinement. This vector type interaction bears a close resemblance to the QCD string, although there are significant differences. We have primarily considered here a class of confinement models that share the same Thomas spin dependence. Our comparison of scalar and string–flux tube confinement has shown some interesting differences and similarities even with spinless quarks. We introduced an intermediate model that has aspects of both scalar confinement and the QCD string. In this intermediate model the energy depends only on the transverse quark velocity as expected in a straight string model. The interaction energy is effectively concentrated at the quark as in scalar potential interaction.

The spin independent relativistic corrections of scalar and

string confinement differ, as has been known for some time [7,8]. The relativistic corrections of the intermediate model are as if an extra transverse mass ar were concentrated at the quarks position. In the string case this same mass is distributed along the string.

It is in the massless limit where interesting distinctions arise. For pure linear scalar confinement the energy of the light degrees of freedom is exactly given by $M^2=2a(J+2n+3/2)$, where J and n are the rotational and radial quantum numbers. The result, shown on the Regge plot in Fig. 1, is a series of straight lines with an excitation pattern $J+2n$. That is, there are degenerate mass towers of states of even or odd parities.

The (laboratory frame) time-component vector confinement again produces linear Regge trajectories, shown in Fig. 2, but with no tower structure, owing to the excitation pattern $J+\sqrt{2}n$ with incommensurate contributions from the rotational and radial quantum numbers. Although one might expect that QCD, being a vector interaction like QED, would have a time-component interaction, it is evidently not time-component in the laboratory frame. This is precisely because the QCD field in which the quark moves is not chromoelectrostatic (purely chromoelectric and time-independent in the laboratory frame). Instead, the QCD field is dynamical because the quark drags a chromoelectric flux tube along with it as it moves. In this respect there are no ''test charges'' in QCD. The QCD field is purely chromoelectric in its rest frame, leading to time-component vector interaction in the quark's rest frame, which we have shown is mathematically equivalent to a scalar interaction. Neglect of the spatial distribution of the QCD field energy thus leads directly to scalar confinement. The string–flux tube picture is the result of taking into account the distribution of the field energy and momentum.

The intermediate model has a Regge structure very different from any of the other models studied here, with somewhat curved trajectories and an uneven pattern of radial excitation, as shown in Fig. 3. Evidently, the modification of the interaction that removes interaction contributions to the radial momentum but leaves all the interaction energy and momentum at the quark's position makes the intermediate model less, rather than more, string-like in its consequences.

The string Regge spectroscopy, Fig. 5, again is similar to that of scalar confinement, except with a different Regge slope. Due to the distribution of energy along the string, the quark now moves at the speed of light in the massless limit. This creates a horizon barrier so the quark appears to move in a half oscillator. The net effect is to give an energy spectrum $M^2=\pi a(J+2n+3/2)$ with the same tower of states structure as in the scalar case. Though the primary difference between the two theories is the manner in which the energy and momentum of the QCD field are distributed, the close relationship between their Regge structures appears to be accidental.

We have pointed out a close, but not exact, relationship between scalar confinement and the QCD string. One might wonder whether one could change the string tension and make the two even more similar. The answer lies in the expectation that the same string tension applies to the Regge slope and to the dynamics of low-lying heavy quark states, i.e., the static potential energy. Both string confinement and scalar confinement reduce to the same linear confinement potential energy for slowly moving heavy quarks. Starting from the universal light hadron Regge slope

$$\alpha' \simeq 0.9 \ \ \mathrm{GeV}^{-2}, \tag{6.1}$$

for mesons consisting of two light quarks the ''slope'' of the static long distance interaction is

$$a_{\mathrm{string}}=\frac{1}{2\pi\alpha'}=0.18 \ \ \mathrm{GeV}^2,$$

$$a_{\mathrm{scalar}}=\frac{1}{4\alpha'}=0.28 \ \ \mathrm{GeV}^2. \tag{6.2}$$

Since these slopes differ by a large ratio, experiment should be able to decide the issue. Heavy quarkonia analyses [20] favor the string tension value over the scalar value in Eq. (6.2).

ACKNOWLEDGMENT

This work was supported in part by the US Department of Energy under Contract No. DE-FG02-95ER40896.

[1] A. B. Henriques, B. H. Kellet, and R. G. Moorhouse, Phys. Lett. **64B**, 85 (1976); H. J. Schnitzer, *ibid.* **65B**, 239 (1976); **69B**, 477 (1977); Phys. Rev. D **18**, 3482 (1978); Lai-Him Chan, Phys. Lett. **71B**, 422 (1977).
[2] N. Isgur, Phys. Rev. D **57**, 4041 (1998).
[3] W. Buchmüller, Phys. Lett. **112B**, 479 (1982).
[4] E. Eichten and F. Feinberg, Phys. Rev. D **23**, 2724 (1981); D. Gromes, Z. Phys. C **22**, 265 (1984); **26**, 401 (1984).
[5] A. Barchielli, E. Montaldi, and G. M. Prosperi, Nucl. Phys. **B296**, 625 (1988); **B303**, 752(E) (1988); A. Barchielli, N. Brambilla, and G. M. Prosperi, Nuovo Cimento A **103**, 59 (1989); N. Brambilla and G. M. Prosperi, Phys. Lett. B **236**, 69 (1990); Phys. Rev. D **46**, 1096 (1992); N. Brambilla, P. Consoli, and G. M. Prosperi, *ibid.* **50**, 5878 (1994); N. Brambilla, A. Pineda, J. Soto, and A. Vairo, ''The QCD potential at $O(1/m)$,'' hep-ph/0002250.
[6] For a different interpretation, see Ken Williams, Phys. Rev. D **59**, 115002 (1999).
[7] N. Brambilla and G. M. Prosperi, Phys. Lett. B **236**, 69 (1990).
[8] Collin Olson, M. G. Olsson, and Ken Williams, Phys. Rev. D **45**, 4307 (1992).
[9] G. S. Bali, S. Schilling, and A. Wachter, Phys. Rev. D **56**, 2566 (1997); G. S. Bali and P. Boyle, *ibid.* **59**, 114504 (1999).
[10] G. S. Bali, ''QCD forces and heavy quark states,'' hep-ph/0001312.

[11] M. G. Olsson, Siniša Veseli, and Ken Williams, Phys. Rev. D **51**, 5079 (1995).
[12] A. Gara, B. Durand, and L. Durand, Phys. Rev. D **40**, 843 (1989).
[13] M. G. Olsson, Siniša Veseli, and Ken Williams, Phys. Rev. D **52**, 5141 (1995).
[14] T. J. Allen, M. G. Olsson, S. Veseli, and K. Williams, Phys. Rev. D **55**, 5408 (1997).
[15] A. Chodos and C. B. Thomas, Nucl. Phys. **B72**, 509 (1974); I. Bars, *ibid.* **B111**, 413 (1976); M. Ida, Prog. Theor. Phys. **59**, 1661 (1978).
[16] R. E. Langer, Phys. Rev. **51**, 669 (1937); M. S. Child, *Molecular Collision Theory* (Academic, New York, 1974).
[17] M. G. Olsson, Phys. Rev. D **55**, 5479 (1997).
[18] M. G. Olsson and S. Veseli, Phys. Rev. D **51**, 3578 (1995).
[19] A. Yu. Dubin and A. B. Kaidalov, Phys. Lett. B **323**, 41 (1994); V. L. Morgunov, A. V. Nefediev, and Yu. A. Simonov, *ibid.* **459**, 653 (1999).
[20] Steve Jacobs, M. G. Olsson, and Casimir Suchyta III, Phys. Rev. D **33**, 3338 (1986).